Early-time photodissociation dynamics of chloroiodomethane in the *A*-band absorption from resonance Raman intensity analysis

Wai Ming Kwok and David Lee Phillips
Department of Chemistry, University of Hong Kong, Pokfulam Road, Hong Kong

We have obtained resonance Raman spectra and absolute Raman cross sections for h_2-chloroiodomethane (fourteen excitation wavelengths between 200 nm and 355 nm) and d_2-chloroiodomethane (for 282.4 nm excitation) in cyclohexane solution. Most of the intensity in the *A*-band resonance Raman spectra appears in the nominal C–I stretch overtones progression and combination bands of the nominal C–I stretch overtones with the fundamentals of the CH_2 wag, CH_2 scissor, and the Cl–C–I bend or C–Cl stretch fundamentals. The *A*-band absorption and absolute resonance Raman intensities were simulated using a simple model which included preresonant contributions to the fundamental Raman peaks and time-dependent wave packet calculations. The motion of the wave packet on the excited state surface was converted from dimensionless normal coordinates into internal coordinates using the results of normal coordinate calculations. The *A*-band short-time photodissociation dynamics of chloroiodomethane shows that the C–I bond lengthens, the I–C–Cl and H–C–I angles become smaller, and the H–C–Cl angles become larger. These internal coordinate motions which are associated with relatively low frequency modes are consistent with a simple impulsive ''soft'' radical model of the photodissociation and the CH_2Cl group changing to a more planar structure. However, the C–H bond length does not change much and the H–C–H angle (associated with higher frequency modes) becomes slightly smaller which is inconsistent with the ''soft'' radical model and the CH_2Cl group changing to a more planar structure. This suggests that an impulsive ''semirigid'' radical model may be more appropriate than the ''soft'' radical model to qualitatively describe the chloroiodomethane photodissociation. An ambiguity in the assignment of the 724 cm^{-1} Raman peak and its associated combination bands to combination bands of the nominal C–I stretch overtones with the fundamentals of the Cl–C–I bend or C–Cl stretch fundamentals limits what we are able to determine about the C–Cl bond length changes during the initial stages of the photodissociation. © *1996 American Institute of Physics.* [S0021-9606(96)01624-8]

I. INTRODUCTION

The development of time-dependent wave-packet theories of resonance Raman scattering by Heller and others[1–5] has made it possible to make an intuitive connection between the vibrational intensities of resonance Raman spectra and the early-time photodissociation dynamics taking place on an excited electronic state potential energy surface in the Franck–Condon region. Over the past decade there have been numerous applications of resonance Raman spectroscopy that examine the photodissociating molecules in terms of a time-dependent approach to resonance Raman scattering.[6–39]

Photodissociation reactions of alkyl halides in their *A*-band absorption have long been studied as prototypes of direct photodissociation reactions. In particular, the photodissociation of iodomethane in the *A*-band absorption has been especially well studied both experimentally and theoretically as a prototype of photodissociation taking place on a directly repulsive potential energy surface. The broad and featureless *A*-band absorption of iodomethane centered near 260 nm is made up of transitions to three different electronic excited states, ${}^3Q_1$, ${}^3Q_0$, and ${}^1Q_1$ as determined from magnetic circular dichroism experiments.[40] The ${}^3Q_0$ transition has approximately 70%–80% of the *A*-band oscillator strength and is located near the *A*-band center. The ${}^3Q_1$ and ${}^1Q_1$ transitions are relatively small and are located on the red and blue edges of the *A*-band absorption. The three *A*-band transitions are all localized on the C–I bond and have $n->\sigma^*$ character. The C–I bond breaks when iodomethane is photoexcited within its *A*-band absorption. The results of photofragment anisotropy measurements have shown that the C–I bond scission is fast compared to the rotational motion of iodomethane[41,42] and the structureless absorption band in the gas phase strongly suggests that the C–I bond breaking is also faster than vibrational recurrence times along any Franck–Condon active bound vibrational mode. Zewail and co-workers have carried out real-time femtosecond pump–probe experiments[43] which found that the photodissociation is complete in less than 100 fs.

Other experiments on the *A*-band photodissociation of iodomethane have investigated the translational energy of the photofragments,[44,45] the vibrational excitation of the methyl fragment,[44,46–50] and the I/I* branching ratio.[51–53] Unlike most alkyl halide *A*-band photodissociation reactions, iodomethane has had a number of vibrational mode-specific techniques applied to examine its photodissociation. A couple of high resolution time-of-flight photofragment spectroscopy experiments[44,45] showed that some internal energy

of the methyl fragment is found in the umbrella mode vibrations. Diode laser absorption,[49] multiphoton ionization (MPI),[46–48] and coherent anti-Stokes Raman scattering[50] experiments have all been used to measure the vibrational and rotational state distributions of the methyl fragment from photodissociation of iodomethane in the A-band. Resonance Raman experiments have been done by several different groups on gas and solution phase iodomethane A-band photodissociation.[7–14] The resonance Raman spectra were dominated by a long overtone progression in the nominal C–I stretch mode with a much smaller combination band progression composed of the nominal CH_3 umbrella mode plus nominal C–I stretch overtones. Several models and potential energy surfaces have been used reasonably successfully to interpret and simulate the wealth of experimental data available for the iodomethane A-band photodissociation[54–61] and it appears that the main features of the A-band photodissociation of iodomethane is fairly well understood.

Chloroiodomethane's A-band absorption band has its peak ~270 nm and an extinction coefficient of about 540 $mol^{-1} L cm^{-1}$ in cyclohexane solution.[62] The absorption spectrum of chloroiodomethane is red shifted and more intense than the corresponding A-band absorption of iodomethane which is ~258 nm and has an extinction coefficient of about 430 $mol^{-1} L cm^{-1}$ in cyclohexane solution. The interaction between the C–Cl and C–I chromophores may be responsible for the red shifting and enhancement of the A-band absorption in chloroiodomethane. Laser flash photolysis experiments performed by Schmitt and Comes[62] on chloroiodomethane have determined that the predominant primary process after photoexcitation in the A-band absorption leads to cleavage of the C–I bond similar to iodomethane and other iodoalkanes.

In contrast to iodomethane, little work has been done to investigate the A-band photodissociation dynamics of dihalomethanes such as chloroiodomethane. Dihalomethanes are interesting since one can examine the interactions between two chromophores as well as investigate bond selective electronic excitation and photochemistry.[63–65] The present paper focuses on the photodissociation of chloroiodomethane in cyclohexane solution. We hope to learn something about the strength of the interaction between the C–Cl and C–I chromophores as well as examine substituent effects on the photodissociation dynamics of iodomethane when one hydrogen atom is replaced with a chlorine atom.

The succeeding sections of the paper will have the following format. Section II will describe the experimental methods used to acquire the resonance Raman spectra of chloroiodomethane in cyclohexane solution. Section III will present the simple model and calculations that are used to model both the absorption spectrum and the absolute resonance Raman intensities. Section IV will describe and discuss the results of the resonance Raman experiments and simulations of the experimental data. Section IV will also present the short-time photodissociation dynamics of chloroiodomethane in the A-band as elucidated from the resonance Raman intensity analysis. Section V will give our conclusions about the A-band photodissociation dynamics of chloroiodomethane.

II. EXPERIMENT

The samples used in the resonance Raman experiments were prepared from spectroscopic grade cylohexane solvent and 99% pure chloroiodomethane purchased from Aldrich Chemical Company or 98% D atom purity d_2-chloroiodomethane purchased from Cambridge Isotope Labs. Solutions of concentrations ranging from 0.10 M to 0.30 M chloroiodomethane in cyclohexane solvent were used in the resonance Raman experiments. The resonance Raman experimental apparatus and methods have been previously published[20,21,32,33] so only a short description will be given here. The excitation frequencies for the Raman experiments were provided by various hydrogen Raman shifted laser lines and the second, third, and fourth harmonics of a Spectra–Physics GCR-150-10 Nd:YAG laser. A loosely focused laser beam ~0.5 mm in diameter and 100–300 μJ excited the flowing liquid sample. An approximately 130° backscattering geometry with laser beam wave vector perpendicular to the scattering plane was used to collect the resonance Raman scattered light. Reflective optics were used in order to avoid or at least minimize chromatic aberrations affecting the relative Raman intensities. An ellipsoidal mirror (Spex with f/1.4) and a flat mirror were used to collect the resonance Raman scattered light and direct it to the entrance slit of 0.5 m spectrograph (Acton) with a 1200 groove/mm ruled grating blaze at 250 nm. A polarization scrambler was mounted on the entrance slit of the spectrograph and a liquid nitrogen cooled Photometrics CCD was mounted on the exit port of the spectrograph. The resonance Raman scattered light passed through the polarization scrambler onto the grating which dispersed the Raman scattered light onto the CCD. The Raman signal was collected for approximately 90 to 300 s before being read out from the CCD detector and to an interfaced PC clone computer system where it was stored as a file on the hard disk. The resonance Raman spectrum was then found by adding up about 10 to 30 of these readout files.

The Raman shifts in wave number of the spectra obtained were calibrated using the known frequencies of the cyclohexane solvent Raman lines. The reabsorption of the resonance Raman scattered light by the strongly absorbing sample was minimized by using a backscattering collection geometry and the remaining reabsorption correction was done using the methods outlined in Refs. 66 and 67. An appropriately scaled solvent spectrum was then subtracted from the reabsorption corrected spectrum in order to delete the solvent lines from the resonance Raman spectra. Spectra of a calibrated intensity deuterium lamp (Optronic model 220M) were recorded and used to correct the resonance Raman spectra for the channel to channel sensitivity of the whole detection system as a function of wavelength. The integrated areas of the resonance Raman peaks were then found by fitting sections of the spectra to a baseline plus a sum of Lorentzian peaks.

The absolute resonance Raman cross sections of chlor-

oiodomethane were measured relative to the previously measured absolute Raman cross sections for the 802 cm^{-1} peak and the C–H stretch vibrational modes near $\sim$2900 cm^{-1} of cyclohexane. The concentrations of the chloroiodomethane/cyclohexane sample solutions were determined spectrophotometrically using a Perkin Elmer 19 UV/VIS spectrometer before and after the Raman measurements. The measured absorption spectra showed changes of 5% or less during the experiment due to evaporation and/or photodecomposition of the sample. The absolute cross section calculations used the average concentrations determined from the initial and final concentrations from a series of measurements at each wavelength. We measured the maximum molar extinction of chloroiodomethane in cyclohexane solution and found it to be 540 M^{-1} cm^{-1}.

III. THEORY AND CALCULATIONS

Usually one assumes that the resonance Raman enhancement for the intensities observed in a resonance Raman spectrum come almost exclusively from the electronic state(s) with which the excitation wavelength is resonant. However, the results presented here for the resonance Raman spectra of chloroiodomethane with excitation in the A-band absorption strongly indicate that preresonance enhancement from higher lying excited states is large enough in the region of the A-band absorption to give rise to preresonance–resonance interference effects in several fundamental resonance Raman intensities. This preresonance–resonance interference causes several of the resonance Raman fundamental peaks to become smaller (de-enhanced) as one tunes the excitation wavelength towards the maximum of the A-band absorption. Since overtones and combination bands decrease in intensity much faster than fundamental bands as the excitation wavelength is moved away from the resonant state, the preresonance–resonance interference effects are largest for fundamental intensities and usually much smaller or negligible for overtones and combination bands in the resonance Raman spectra. Preresonance–resonance interference effects have been observed experimentally in the excitation profiles of a number of molecules over the past 20 years by several different research groups.[30,68–74] Preresonance–resonance interference effects have also been successfully modeled and elucidated theoretically.[30,68–74]

The procedure for modeling the absorption and absolute resonance Raman intensities of chloroiodomethane in the A-band absorption closely follows that used by Phillips and Myers[30] to model the A-band absolute resonance Raman intensities of several alkyl iodides. The preresonant contribution was estimated by fitting the absolute resonance Raman intensities in the 204 nm to 223 nm region (to the blue of the A-band absorption) to a single-state A-term frequency dependence[75] given by Eqs. (1) and (2),

$$\sigma_R(E_L) = E_L E_S^3 [A_{pre}]^2 \qquad (1)$$

and

$$[A_{pre}]^2 = K[(E_e^2 + E_L^2)/(E_e^2 - E_L^2)^2]^2, \qquad (2)$$

where E_L and E_S are the laser and scattered photon energies, K is the coupling strength, and E_e is the resonant state energy. The preresonant data were fit using Eqs. (1) and (2) and allowing K and E_e to vary to give the best overall fit to the 208.8 nm, 217.8 nm, and 223.1 nm absolute Raman cross sections. Since there are many electronic excited states with large oscillator strengths in the quasicontinuum absorption below 200 nm, it is very probable that a single state A-term dependence will not adequately describe the energy dependence of the preresonant Raman intensities over a large range of excitation energies. Therefore, the extrapolation of the preresonant contribution in the A-band from the A-term fit was used as a initial approximation that was changed moderately in simulating the A-band absolute resonance Raman intensities.

The A-band absorption spectrum and resonance Raman intensities were simulated using time-dependent wave packet calculations which included the preresonant contribution to the Raman amplitude. The absorption spectrum was calculated using the following equation:

$$\sigma_A(E_L) = (4\pi e^2 E_L M^2/3n\hbar^2 c) \mathrm{Re} \int_0^\infty \langle 0|0(t)\rangle$$

$$\times \exp[i(E_L + \epsilon_0)t/\hbar], \qquad (3)$$

where E_L is the incident photon energy, n is the solvent index of refraction, ϵ_0 is the ground-state zero-point vibrational energy, M is the transition length evaluated at the equilibrium geometry, $|0(t)\rangle = e^{-iHt/\hbar}|0\rangle$ which is $|0(t)\rangle$ propagated on the excited state surface for a time t, and H is the excited state vibrational Hamiltonian. The very fast damping of the overlaps by wave packet motion out of the Franck–Condon region alone led us to use no extra damping due to another population decay pathway or pure dephasing decay. Only the vibrational ground-state ($v=0$) was taken into account in the calculations. The resonance Raman intensity simulations assume that the resonant amplitude comes from only one electronic state. However, the A-band absorption of chloroiodomethane is probably composed of transitions to three electronic states similar to the A-band absorption of iodomethane. Magnetic circular dichroism experiments by Rowe and Gedanken[40] showed that the A-band absorption of iodomethane is dominated by the $^3Q_0$ state which has 70%–80% of the oscillator strength. We expect that the A-band absorption of chloroiodomethane is similarly dominated by the $^3Q_0$ state and the smaller transitions have been left out to keep the calculations fairly simple. When more than one electronic transition contributes to the resonance Raman intensities, the different electronic transition contributions are first summed up at the amplitude level and then squared. The leading additional contributions from the smaller transitions will be their cross terms with the strongest electronic transition and the smaller transition contribution will scale close to linear relative to the largest electronic band (ignoring coupling strengths). In regions of the absorption band where the $^3Q_0$ transition does not dominate and the smaller transitions make more significant contributions, leaving out the smaller transitions from the calcula-

tions can lead to some error in the calculated resonance Raman intensities and this is discussed more fully in Sec. IV. However, for regions of the A-band absorption where the $^3Q_0$ transition dominates we would expect that the assumption that the resonant contribution to the resonance Raman intensities comes from a single electronic state to be a reasonably good approximation.

The interference between the preresonant and resonant amplitudes depends on whether the two amplitudes contribute to the same or to different tensor elements of the Raman polarizability. We will treat chloroiodomethane as a cylindrical molecule since the largest electronic transition ($^3Q_0$) of the A-band absorption is mostly localized on the C–I bond. For a diatomic molecule such as iodine it is possible to choose the molecule-fixed coordinate system to diagonalize the polarizability tensor α. However, this is not generally possible for the general resonance Raman polarizability tensor since it does not need to be symmetric. If the dominant A-band absorption transition is localized on the C–I bond so that it can be thought of as being very close to diatomic in character then we expect that an appropriate choice of the molecule-fixed coordinate system will lead to the polarizability tensor being dominated by the diagonal terms. The nondiagonal elements ($\alpha_{\gamma\beta}$) can then be thought of as a measure of the non C–I character of the A-band transitions. Since the A-band absorption of chloroiodomethane and iodomethane are very similar to one another in both shape and transition strength and the iodomethane A-band transitions are almost entirely localized along the C–I bond, we expect that the largest A-band transitions of chloroiodomethane to be dominated by the diagonal polarizability elements and the off diagonal polarizability elements ($\alpha_{\gamma\beta}$) to be relatively small. For simplicity, we will assume that the $^3Q_0$ transition of the chloroiodomethane A-band absorption is entirely localized on the C–I bond. Using the preceding assumption, we have only two tensor elements to consider for the Raman polarizability, $\alpha_{\gamma\gamma}$ and $\alpha_{\beta\beta}$, where γ is the symmetry axis and β is the doubly degenerate axes. Our experiment measures the differential Raman cross section as given in Eq. (4) in terms of $\alpha_{\beta\beta}$ and $\alpha_{\gamma\gamma}$,

$$(d\sigma/d\Omega)_{\parallel+\perp} = (4E_S^3 E_L)/[15(\hbar c)^4][|\alpha_{\gamma\gamma}|^2$$
$$+ (9/4)|\alpha_{\beta\beta}|^2 + (1/4)$$
$$\times (\alpha_{\gamma\gamma}^* \alpha_{\beta\beta} + \alpha_{\beta\beta}^* \alpha_{\gamma\gamma})]. \quad (4)$$

Integrating over all directions and polarizations of the Raman scattering gives the total Raman cross section as shown in Eq. (5),

$$\sigma_T(E_L, E_S) = (8\pi/3)[(1+2\rho)/(1+\rho)](d\sigma/d\Omega)_{\parallel+\perp}, \quad (5)$$

where ρ is the depolarization ratio as listed below in terms of $\alpha_{\beta\beta}$ and $\alpha_{\gamma\gamma}$ in Eq. (6),

$$\rho = [|\alpha_{\gamma\gamma}|^2 + |\alpha_{\beta\beta}|^2 - (\alpha_{\gamma\gamma}^* \alpha_{\beta\beta} + \alpha_{\beta\beta}^* \alpha_{\gamma\gamma})]/[3|\alpha_{\gamma\gamma}|^2$$
$$+ 8|\alpha_{\beta\beta}|^2 + 2(\alpha_{\gamma\gamma}^* \alpha_{\beta\beta} + \alpha_{\beta\beta}^* \alpha_{\gamma\gamma})]. \quad (6)$$

The depolarization ratio will usually be a function of excitation wavelength due to the frequency dependence of $\alpha_{\beta\beta}$ and $\alpha_{\gamma\gamma}$. Phillips and Myers[30] previously examined two cases for the preresonant–resonant interference of A-band resonance Raman fundamentals of several alkyl iodides. The first case investigated when the higher lying electronic states are polarized predominantly along the C–I bond then both the resonant and preresonant parts only contribute to $\alpha_{\gamma\gamma}$. The second case examined when the higher lying electronic states are polarized perpendicular to the C–I bond which leads to the preresonant Raman amplitude contributing only to the $\alpha_{\beta\beta}$ tensor component. The preresonant–resonant interference cross terms are substantially smaller for the second case where the higher states are polarized perpendicular to the C–I and Phillips and Myers[30] found that the interference effect was too small to account for the experimentally observed excitation profiles for the affected fundamental resonance Raman intensities whether an A-term or B-term frequency dependence is used for the preresonant contribution. However, when the preresonant contribution was assumed to be primarily from electronic states with their transitions polarized parallel to the C–I bond then resonance Raman fundamental intensities could be fit very well. These results indicate that the primary electronic states responsible for the preresonant contribution have transitions polarized parallel to the C–I bond for the alkyl iodides (iodomethane, iodoethane, 2-iodopropane, and tert-butyl iodide).

Since chloroiodomethane is very similar to the alkyl iodides we will assume that the higher electronic states giving the dominant contributions to the preresonant contributions in the A-band also have their transitions polarized parallel to the C–I bond. Using the assumption that the preresonant contribution is from electronic states whose transitions are parallel to the C–I bond, the depolarization ratio will become 1/3 independent of excitation frequency and the experimentally measured differential Raman cross section (for our experimental geometry) is given by

$$(d\sigma/d\Omega)_{\parallel+\perp} = (4E_S^3 E_L)/[15(\hbar c)^4]|\alpha_{\text{res}} + \alpha_{\text{pre}}|^2. \quad (7)$$

The total Raman cross section is then given by

$$\sigma_I(E_L, E_S) = (10\pi/3)(d\sigma/d\Omega)_{\parallel+\perp}. \quad (8)$$

The resonant Raman amplitude is calculated using Eq. (9),

$$\alpha_{\text{res}} = (e^2 M^2/\hbar) \int_0^\infty \langle f|0(t)\rangle \exp[i(E_L + \epsilon_0)t/\hbar]dt, \quad (9)$$

and the preresonant Raman amplitude is given by Eq. (10),

$$|\alpha_{\text{pre}}|^2 = [9(\hbar c)^4/8\pi][A_{\text{pre}}]^2. \quad (10)$$

The preresonant contribution was assumed to be negligible for all combination bands and overtones which were found to be weak in the Raman spectra taken in the 208.8–223.1 nm region and for any fundamental that was also found to have a small intensity in the 208.0 nm to 223.1 nm region. Since the resonant Raman amplitude given in Eq. (9) approaches a pure imaginary form as it is tuned away from resonance, we have given the preresonant contribution a pure imaginary form. The resonant and preresonant contribution relative

TABLE I. Chloroiodomethane ground state normal modes.

	h_2-chloroiodomethane		d_2-chloroiodomethane	
Mode	Experiment[a] frequency (cm^{-1})	Calculated frequency (cm^{-1})	Experiment[b] frequency (cm^{-1})	Calculated frequency (cm^{-1})
ν_1	2978	2992.6	2190	2172.9
ν_2	1392	1394.7	1029	1036.2
ν_3	1183	1184.6	896	888.7
ν_4	720	718.9	701	694.2
ν_5	531	535.4	503	497.0
ν_6	196	195.0	197	194.3
ν_7	3050	3071.8	2303	2276.5
ν_8	1108	1113.0	801	793.4
ν_9	789	791.9	615	618.8

[a]Frequencies are from the Raman peaks observed in Ref. 80.
[b]Frequencies are from the Raman peaks observed in Ref. 79.

signs depend on the relative direction of the geometry change along the particular normal mode vibration of interest in the excited electronic states that give rise to the resonant and preresonant contributions. We have assumed that the direction of the geometry change along each normal coordinate is the same in both the resonant and preresonant excited states and this will give the resonant and preresonant terms the same signs. This will probably be a good approximation for the nominal C–I stretch which will most likely increase in bond length in almost all of its excited states. We have scaled the magnitude of the preresonant contribution by an overall factor ranging from 0.6 to 1.2 to best fit the A-band resonance Raman fundamental intensities in our calculations because the single state A-term fit approximation used to find the preresonant contributions is a rough guide and not an exact description.

The ground and excited electronic state potential energy surfaces were modeled as harmonic oscillators with their minima separated by a displacement, Δ, given in dimensionless ground-state normal coordinates. The ground and excited state harmonic oscillators were assumed to have the same frequency and the model had no Duchinsky rotation of the normal coordinate. When no vibrational recurrences are allowed, the absorption spectrum and resonance Raman intensities of the first few overtones and combination bands are determined mostly by the slope of the Franck–Condon region excited state potential energy surface. The broad and featureless gas and solution phase absorption spectra of chloroiodomethane imply that the total electronic dephasing is probably mainly due to photodissociation before the first vibrational recurrence. Excited state population decay (due to photodissociation) and/or electronic pure dephasing were mimicked by truncating the time integral of Eqs. (3) and (9) at a time after the wave packet has moved far enough from zero time so that their is no longer significant overlap between the wave packet and the final states making up the resonance Raman spectrum. Therefore, our simple harmonic oscillator model for the excited state potential energy surface only gives us a convenient method with which to simulate the segment of the excited state surface in the Franck–Condon region that accounts for the observed absorption

spectrum and resonance Raman intensities and does not in any way suggest that the excited state is actually bound. The multidimensional slope of the excited state potential energy surface and the associated early-time nuclear dynamics are well determined by our simple model in the Franck–Condon region, but our model parameters cannot be counted on to determine anything about the dynamics outside the excited state Franck–Condon region.

The parameters used in the model described above are typically given in terms of dimensionless normal coordinates. To elucidate the short-time photodissociation dynamics in terms of actual atomic displacements we need to convert the motion of the center of the wave packet from being described in ground-state dimensionless normal coordinates to being described in internal coordinates using the normal-mode vectors from normal coordinate calculations. The normal mode-vectors for fully protonated and deuterated chloroiodomethane were calculated with an adapted version of the Snyder and Schachtschneider FG program[76] and used previously published ground-state geometries from microwave spectroscopy experiments[77] and valence force fields for fully
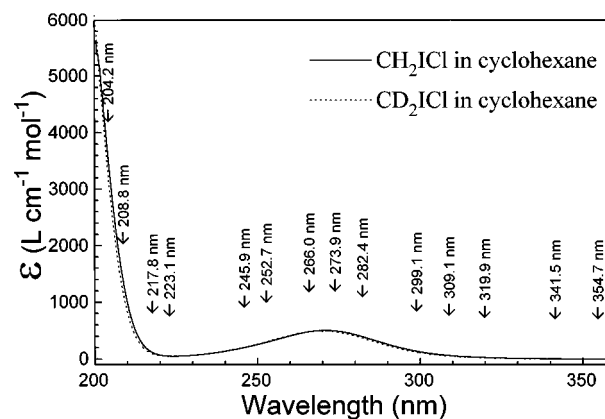

FIG. 1. Fully protonated and deuterated chloroiodomethane in cyclohexane solution absorption spectra. The excitation wavelengths for the resonance Raman spectra are shown by the arrows and numbers (in nm) above the absorption spectra.
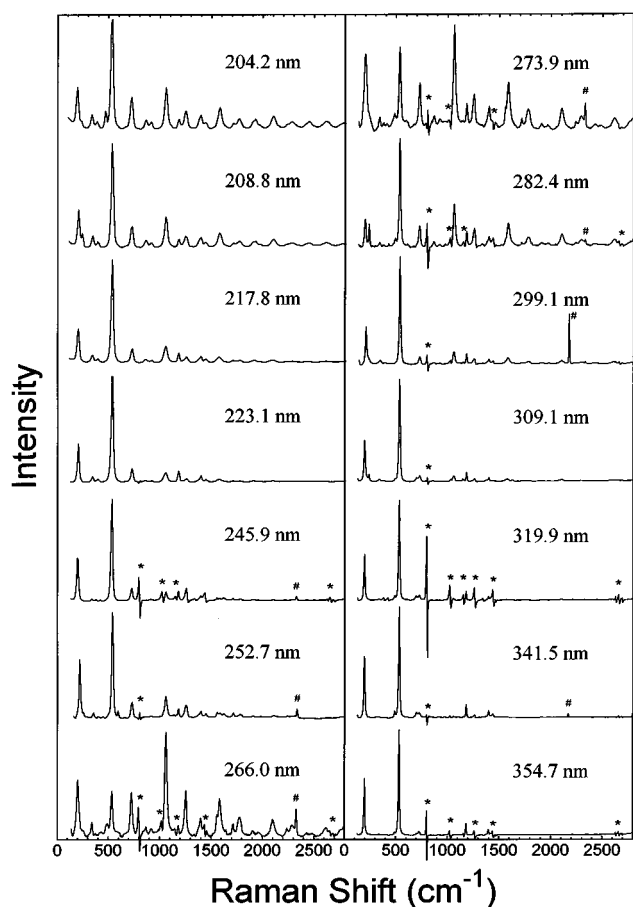
FIG. 2. Overview of the chloroiodomethane in cyclohexane solution resonance Raman spectra. The spectra have been intensity corrected and solvent subtracted. The asterisks (*) mark solvent subtraction artifacts and the pound sign (#) marks a laser line artifact.

protonated chloroiodomethane.[78(a)] The previously published valence force fields have been changed slightly to give a better overall fit to the experimental frequencies of both the fully protonated and deuterated chloroiodomethane.[79,80] The complete force field, Cartesian coordinates, computed vibrational frequencies, and normal-mode coefficients are available as supplementary material.[78(b)] Table I shows the calculated and experimental vibrational frequencies of fully protonated and deuterated chloroiodomethane.

The center of the wave packet position at time t after excitation and experiencing separable harmonic motion is expressed in dimensionless normal coordinates as

$$q_\alpha(t) = \Delta_\alpha(1 - \cos \omega_\alpha t), \qquad (11)$$

where $q_\alpha = 0$ for each mode α at the ground-state equilibrium geometry, ω_α is the vibrational frequency in fs^{-1}, and ϖ_α is the vibrational frequency in cm^{-1}. The dimensionless displacements of Eq. (11) are given in terms of the internal coordinates by

$$s_i(t) = (h/2\pi c)^{1/2}\Sigma_\alpha A_{\alpha i}\varpi_\alpha^{-1/2}q_\alpha(t), \qquad (12)$$

where s_i are the internal coordinate (Wilson, Decius, and Cross defined stretches, bends, wags, and torsions)[81] dis-

placements from their ground-state equilibrium values, $A_{\alpha i}$ is the normal-mode coefficient $(\partial s_i/\partial Q_\alpha)$, found from the normal coordinate calculations, and Q_α is the ordinary normal coordinate.

IV. RESULTS AND DISCUSSION

A. Absorption spectrum

The absorption spectra of h_2-chloroiodomethane and d_2-chloroiodomethane in cyclohexane solvent are shown in Fig. 1. The excitation wavelengths for the resonance Raman experiments are displayed as numbers (in nm) above the chloroiodomethane spectrum. The chloroiodomethane spectrum (maximum ~270 nm and ϵ=540 mol^{-1} L cm^{-1}) is red-shifted and more intense than that of iodomethane (maximum ~258 nm and ϵ=430 mol^{-1} L cm^{-1}). The A-band of iodomethane (and presumably chloroiodomethane) is made up of three $n\rightarrow\sigma^*$ transitions to directly dissociative states ($^3Q_0$, $^1Q_1$, and $^3Q_1$) with the $^3Q_0$ transition having most of the oscillator strength (~70%–80%) of the iodomethane A-band absorption. Substitution of a hydrogen atom on iodomethane with a chlorine atom gives noticeable changes in the absorption spectrum and may result in some differences in the relative strengths of the three dissociative transitions in chloroiodomethane compared to iodomethane.

B. Resonance Raman spectra

Figure 2 displays an overview of the A-band resonance and postresonance Raman spectra of chloroiodomethane in cyclohexane solution and Fig. 3 presents a larger view of the 282.4 mm chloroiodomethane resonance Raman spectrum. The spectra shown in Figs. 2 and 3 have been corrected for reabsorption and the detection system wavelength dependent sensitivity as well as solvent subtracted. The solvent subtraction of the very strong C–H stretch peaks around 2800–3100 cm^{-1} makes that part of the spectrum very noisy and this region is not shown. The low frequency region of the spectra
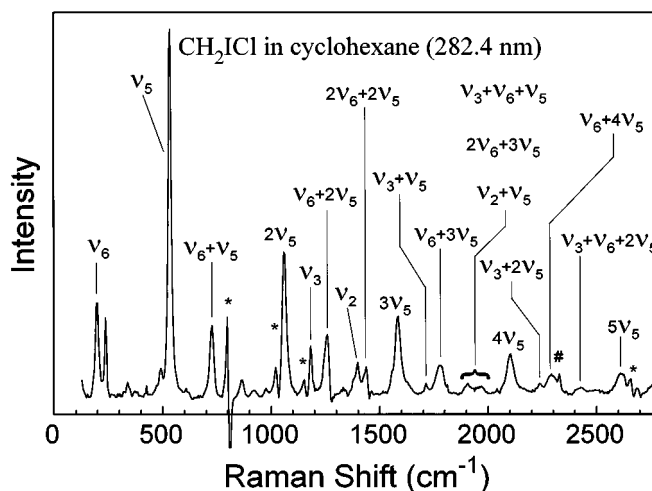

FIG. 3. A larger view of a typical A-band resonance Raman spectrum (282.4 nm spectrum is shown). The spectrum has been intensity corrected and solvent subtracted. The assignments of the larger Raman peaks have been labeled. The asterisks (*) mark solvent subtraction artifacts.

TABLE II. Resonance Raman intensities of chloroiodomethane in cyclohexane solution.

Raman peak[a]	Raman shift[b]	309.1 nm intensity[c]	299.1 nm intensity	282.4 nm intensity	273.9 nm intensity	266.0 nm intensity	252.7 nm intensity	245.9 nm intensity
ν_5	532	1004	585	208	67	38	362	1320
$2\nu_5$	1061	100	100	100	100	100	100	100
$3\nu_5$	1583	61	81	84	71	67	23	34
$4\nu_5$	2101	48	47	50	36	29	10	13
$5\nu_5$	2614	46	42	41	25	19	⋯	⋯
$\nu_4(\nu_6+\nu_5)$	725	71	64	48	42	42	70	183
$\nu_4+\nu_5(\nu_6+2\nu_5)$	1255	40	38	46	31	46	60	167
$\nu_4+2\nu_5(\nu_6+3\nu_5)$	1777	14	37	40	36	32	20	26
$\nu_4+3\nu_5(\nu_6+4\nu_5)$	2293	25	24	31	27	26	17	44
$2\nu_4(2\nu_6+2\nu_5)$	1435	13	14	14		5	12	74
$2\nu_4+\nu_5(2\nu_6+3\nu_5)$	1962	8	6	11	7	5	4	28
$\nu_4+\nu_6(\nu_5+2\nu_6)$	921	9	10	6	4	3	6	15
ν_3	1183	67	44	19	12	⋯	23	86
$\nu_3+\nu_5$	1713	4	7	4	6	9	15	21
$\nu_3+2\nu_5$	2237	7	4	6	4	6	8	⋯
$\nu_3+\nu_4,\ \nu_2+\nu_5$ $(\nu_3+\nu_6+\nu_5)$	1905	15	15	10	7	7	4	11
$\nu_3+\nu_4+\nu_5,\ \nu_2+2\nu_5$ $(\nu_3+\nu_6+2\nu_5)$	2424	⋯	13	7	7	5	⋯	13
ν_2	1396	47	40	30	23	20	30	140
$\nu_9+\nu$	1331	⋯	⋯	4	⋯	1	⋯	59
ν_6	190	428	214	61	117[d]	71[d]	189	566

[a]Alternative assignment of $(\nu_6+\nu_5)$ for (ν_4) is given in parentheses.
[b]Estimated uncertainties are about ± 4 cm^{-1} for the Raman shifts.
[c]Relative intensities are based on integrated areas of peaks. Estimated uncertainties are about 10% for intensities 50 and higher, 20% for intensities 10–50, and 30% for intensities lower than 10.
[d]Subtraction of large Rayleigh background and solvent peaks make features below 500 cm^{-1} unreliable in the 273.9 nm and 266.0 nm spectra.

has had the red-edge wing of the Rayleigh laser line subtracted from the spectra. The resonance Raman spectra taken near the peak of the A-band absorption have a relatively large Rayleigh light background in the frequency region below 500 cm^{-1} Raman shift with a substantial solvent subtraction of the 436 and 343 cm^{-1} solvent lines which also make this region of the spectra relatively noisy and therefore this region spectral features are not very reliable in the 266.0 nm, 273.9 nm, 282.4 nm, and 299.1 nm spectra. The larger Raman peaks labeled in Fig. 3 have been tentatively assigned based on published nonresonant Raman spectra and the pre-resonant Raman spectra reported in this work. The fundamentals, overtones, and combination bands of four (or five) Franck–Condon active vibrational modes comprise most of the Raman intensity in the spectra of Figs. 2 and 3. The largest progression of Raman peaks are the fundamental and overtones of the nominal C–I stretch ($n\nu_5$) and we observe ν_5, $2\nu_5$, $3\nu_5$, $4\nu_5$, and $5\nu_5$. These C–I stretch bands ($n\nu_5$) also form noticeable combination bands with the CH$_2$ wag (ν_3) and CH$_2$ scissor (ν_2) fundamentals, $\nu_3+\nu_5$, $\nu_3+2\nu_5$, and $\nu_2+\nu_5$. The near degeneracy of the ν_4 and the $\nu_6+\nu_5$ peaks makes the assignment of the 724 cm^{-1} Raman peak and the combination bands associated with it difficult.

In our preliminary work[32] we observed two features around 700–724 cm^{-1} in the resonance Raman spectra with excitation wavelengths between 355 nm and 309 nm. Further work on chloroiodomethane has determined that the second Raman peak around 700 cm^{-1} is due to the $\nu_9+\nu_4$ peak of the diiodomethane[20,21] impurity in the chloroiodomethane

sample. Although the diiodomethane impurity is <1% in the chloroiodomethane sample, diiodomethane has a substantially larger absorption cross section between 300 nm to 350 nm region compared to chloroiodomethane which leads to the diiodomethane peaks being resonantly enhanced strongly in this region. The largest line in the diiodomethane/cyclohexane spectrum is the $\nu_9+\nu_4$ peak at 703 cm^{-1} and this shows up as a small feature in the chloroiodomethane spectra with excitation wavelengths between 309 nm and 355 nm. The diiodomethane impurity also has a noticeable feature near 493 cm^{-1} due to the fundamental of the C–I stretch (ν_3) and this peak appears in several chloroiodomethane spectra as a very small shoulder of the very large chloroiodomethane C–I stretch fundamental. The other Raman peaks in the diiodomethane spectra[20,21] between 180–2500 cm^{-1} are substantially smaller than the $\nu_9+\nu_4$ and the ν_3 peaks and do not appear to have significant contributions to the resonance Raman spectra of chloroiodomethane.

Nonresonant Raman spectra are usually dominated by fundamental Raman lines since overtones and combination bands are expected to be weak far from resonance. However, combination bands and overtones can have noticeable intensity in nonresonant Raman spectra. The nonresonant Raman spectra obtained by Klaboe and co-workers[80] show peaks that they have assigned to the overtones and combination bands of the nominal C–I stretch and the nominal Cl–C–I bend; ν_5 at 531 cm^{-1}, $2\nu_5$ at 1056 cm^{-1}, ν_6 at 196 cm^{-1}, $2\nu_6$ at 393 cm^{-1}, and $\nu_5-\nu_6$ at 333 cm^{-1}. The 720 cm^{-1} feature that Klaboe and co-workers[80] assigned to (ν_4) the nominal
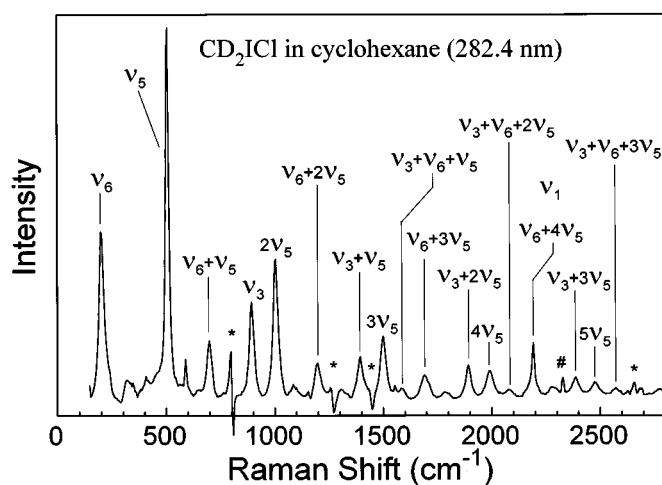
FIG. 4. Resonance Raman spectrum of d_2-chloroiodomethane taken with 282.4 nm excitation. The spectrum has been intensity corrected and solvent subtracted. The assignments of the larger Raman peaks have been labeled. The asterisks (∗) mark solvent subtraction artifacts.

C–Cl stretch fundamental could have some intensity from the combination band $(\nu_5+\nu_6)$ of the two strongest fundamentals observed in the nonresonant spectra chloroiodomethane especially since the difference band $(\nu_5-\nu_6)$ of those fundamentals has noticeable intensity. The 724 cm^{-1} peak observed in our resonance Raman spectra may have significant contributions from both the ν_4 and the $\nu_6+\nu_5$ peaks. Since we cannot rule out that the 724 cm^{-1} peak is predominately either ν_4 or $\nu_6+\nu_5$, we will analyze and discuss both possible assignments in the succeeding sections. Table II lists the experimental resonance Raman positions and intensities for the excitation wavelengths in the A-band with the alternative peak assignments listed in parentheses.

Figure 4 shows the resonance Raman spectrum of fully deuterated chloroiodomethane taken with a 282.4 nm excitation wavelength. The 282.4 nm resonance Raman spectrum of deuterated chloroiodomethane has fundamentals, overtones, and/or combination bands of three (or four) Franck–Condon active modes. Similar to the fully protonated spectra the largest progression of Raman peaks are the fundamental and overtones of the nominal C–I stretch $(n\nu_5)$ progression $(\nu_5, 2\nu_5, 3\nu_5, 4\nu_5,$ and $5\nu_5)$. These C–I stretch bands $(n\nu_5)$ also form combination bands with the CH$_2$ wag (ν_3) fundamental, $\nu_3+\nu_5$, $\nu_3+2\nu_5$, and $\nu_3+3\nu_5$. Since the near degeneracy of the ν_4 and the $\nu_6+\nu_5$ peaks is not removed by deuteration, the 697 cm^{-1} Raman peak and the combination bands associated with it are nominally assigned as ν_4 and $\nu_4+n\nu_5$ peaks with the alternative assignment as the $\nu_6+n\nu_5$ series of peaks similar to what we have done with the protonated chloroiodomethane spectral assignments. Comparison of the h_2-chloroiodomethane and d_2-chloroiodomethane resonance Raman spectra (Figs. 2–4) shows that the CH$_2$ wag (ν_3) fundamental and its combination bands with the nominal C–I stretch $(\nu_3+n\nu_5)$ become more intense in the deuterated spectra. Table III gives the Raman shifts and rela-

TABLE III. Resonance Raman intensities of deuterated chloroiodomethane in cyclohexane solution obtained with 282.4 nm excitation.

Raman peak[a]	Raman shift (cm^{-1})[b]	282.4 nm intensity[c]
ν_5	505	165
$2\nu_5$	1004	100
$3\nu_5$	1499	52
$4\nu_5$	1991	25
$5\nu_5$	2476	12
$\nu_4(\nu_6+\nu_5)$	697	43
$\nu_4+\nu_5(\nu_6+2\nu_5)$	1196	29
$\nu_4+2\nu_5(\nu_6+3\nu_5)$	1691	28
$\nu_4+3\nu_5(\nu_6+4\nu_5)$ and ν_1	2191	25[d]
ν_3	892	70
$\nu_3+\nu_5$	1393	39
$\nu_3+2\nu_5$	1891	22
$\nu_3+3\nu_5$	2385	15
$\nu_3+\nu_4$ ($\nu_3+\nu_6+\nu_5$)	1586	10
$\nu_3+\nu_4+\nu_5$ ($\nu_3+\nu_6+2\nu_5$)	2079	4
$\nu_3+\nu_4+2\nu_5$ ($\nu_3+\nu_6+3\nu_5$)	2572	5
ν_6	191	131

[a]Alternative assignment of $(\nu_6+\nu_5)$ for (ν_4) is given in parentheses.
[b]Estimated uncertainties are about ±4 cm^{-1} for the Raman shifts.
[c]Relative intensities are based on integrated areas of peaks. Estimated uncertainties are about 10% for intensities 50 and higher, 20% for intensities 10–50, and 30% for intensities lower than 10.
[d]Two peaks contribute to this intensity (the nominal C–D stretch, ν_1, and either $\nu_4+3\nu_5$ or $\nu_6+4\nu_5$).

tive intensities for the 282.4 nm deuterated chloroiodomethane resonance Raman spectrum.

C. Resonance Raman absolute cross sections

The measured absolute Raman cross sections for the nominal C–I stretch (ν_5) fundamental for chloroiodomethane at the wavelengths given in Fig. 2 are shown in Table IV. The measured relative differential Raman cross sections were converted into absolute cross sections using Eq. (5) and depolarization ratios of 0.10 for the 802 cm^{-1} cyclohexane

TABLE IV. Nominal C–I stretch fundamental absolute Raman cross sections for h_2-chloroiodomethane.

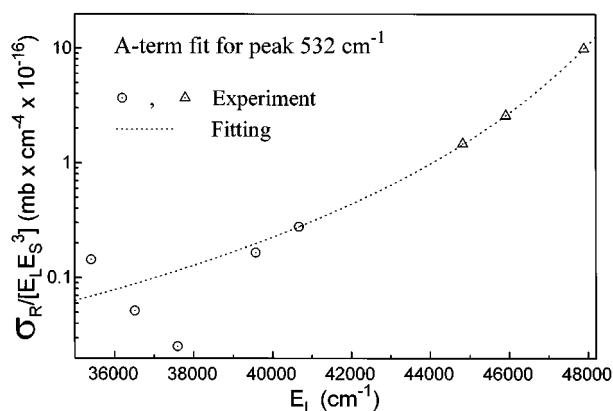| Wavelength	Absolute cross section (Å^2/molecule)
204.2 nm	9.6×10^{-8}
208.8 nm	5.1×10^{-8}
217.8 nm	1.1×10^{-8}
223.1 nm	5.7×10^{-9}
245.9 nm	7.3×10^{-10}
252.7 nm	3.9×10^{-10}
266.0 nm	4.9×10^{-11}
273.9 nm	8.8×10^{-11}
282.4 nm	2.2×10^{-10}
299.1 nm	2.2×10^{-10}
309.1 nm	1.6×10^{-10}
319.9 nm	9.2×10^{-11}
341.5 nm	4.3×10^{-11}
354.7 nm	3.6×10^{-11}

FIG. 5. Extrapolation of the A-term fit (dashed line) from the preresonant absolute Raman cross sections (triangles) of the ν_5 nominal C–I stretch fundamental into the A-band region and a comparison to the experimentally observed ν_5 nominal C–I stretch fundamental absolute Raman cross sections in the A-band region (circles).

peak, 0.23 for the sum of the C–H stretches of cyclohexane, and an assumption of 0.33 for the chloroiodomethane peaks. Examination of Table IV shows that absolute Raman cross sections with excitation wavelengths from 204.2 nm to 223.1 nm preresonant to the B-band are much higher than those with excitation wavelengths in the A-band. Figure 5 shows an A-term fit to the 208.8 nm, 217.8 nm, and 223.1 nm nominal C–I stretch fundamental absolute cross section and an extrapolation of the fit to the A-band region where it is compared to the observed Raman cross sections. Figure 5 clearly shows that the preresonant contribution from higher lying electronic states is comparable to the actual intensity observed in the A-band resonance Raman spectra. Thus, the preresonant contribution cannot be ignored when modeling the fundamental intensities of the A-band resonance Raman spectra.

D. Simulations of resonance Raman intensities and absorption spectra

We have simulated the A-band absorption spectra and resonance Raman absolute cross sections taking into account the preresonant contribution and using Eqs. (2)–(10). The excitation wavelengths near the center of the A-band were weighted more than the red and blue edge spectra when determining the normal mode-displacement parameters that best fit the overtone and combination band resonance Raman intensities. However all of the excitation wavelengths were given equal weighting when adjusting the preresonance contribution (0.6 to 1.2 of the A-term fit described in Sec. III) to best fit the excitation profile of the fundamental intensities. Table V shows the parameters used in calculating the A-band absorption spectra and resonance Raman intensities for h_2-chloroiodomethane. Tables VI and VII compare the calculated relative resonance Raman intensities to the experimental intensities while Fig. 6 shows a typical graphical comparison for 282.4 nm. In general, there is reasonable agreement between the calculated and experimental relative resonance Raman intensities at excitation wavelengths near the center and red edges of the A-band absorptions. There appears to be noticeably worse agreement between experiment and calculated intensities at excitation wavelengths near the blue edge of the A-band absorption (see Tables VI and VII). The $^1Q_1$ state is likely to significantly perturb the resonance Raman intensities near the blue-edge of the A-band and lead to disagreement between the experimental intensities and our calculated Raman intensities which neglects the presence of the $^1Q_1$ state. Tables VI and VII also compare the experimental and calculated absolute resonance Raman cross section for the first overtone of the nominal C–I stretch ($2\nu_5$). The agreement of the experimental and calculated absolute Raman cross sections for the first overtone of the nominal C–I stretch ($2\nu_5$) is excellent for most

TABLE V. Parameters for calculation of resonance Raman intensities and absorption spectrum of chloroiodomethane in cyclohexane solution.

Vibrational mode	Ground state vibrational frequency (cm^{-1})	Excited state vibrational frequency (cm^{-1})	$|\Delta|$
(a) Using assignment of 724 cm^{-1} peak to ν_4			
ν_5 (C–I stretch)	532 cm^{-1}	532 cm^{-1}	4.9
ν_4 (C–Cl stretch)	725 cm^{-1}	725 cm^{-1}	1.62
ν_3 (CH$_2$ wag)	1183 cm^{-1}	1183 cm^{-1}	0.48
ν_2 (CH$_2$ scissor)	1396 cm^{-1}	1396 cm^{-1}	0.15
ν_9 (CH$_2$ twist)	800 cm^{-1}	800 cm^{-1}	0.47
ν_6 (Cl–C–I bend)	190 cm^{-1}	190 cm^{-1}	0.50
Transition length, $M=0.186$ Å			
$E_0=29\,520$ cm^{-1}			
(b) Using assignment of 724 cm^{-1} peak to $\nu_5+\nu_6$			
ν_5 (C–I stretch)	532 cm^{-1}	532 cm^{-1}	4.9
ν_6 (Cl–C–I bend)	190 cm^{-1}	190 cm^{-1}	6.0
ν_3 (CH$_2$ wag)	1183 cm^{-1}	1183 cm^{-1}	0.48
ν_2 (CH$_2$ scissor)	1396 cm^{-1}	1396 cm^{-1}	0.22
ν_9 (CH$_2$ twist)	800 cm^{-1}	800 cm^{-1}	0.47
Transition length, $M=0.186$ Å			
$E_0=27\,030$ cm^{-1}			

TABLE VI. Comparison of experimental and calculated resonance Raman intensities of chloroiodomethane in cyclohexane solution using the assignment of the 724 cm^{-1} peak to ν_4.

Raman peak[a]	Raman shift[b]	282.4 nm		273.9 nm		266.0 nm	
		Expt.[c]	Calc.	Expt.	Calc.	Expt.	Calc.
(a) Excitation wavelengths at center of A-band absorption spectrum							
ν_5	532	208	129	67	36	38	20
$2\nu_5$	1061	100	100	100	100	100	100
Absolute Raman cross section for $2\nu_5$ in Å^2/molecule (Calc)		1.04×10^{-10} (9.83×10^{-11})		1.31×10^{-10} (1.31×10^{-10})		1.28×10^{-10} (1.35×10^{-10})	
$3\nu_5$	1583	84	65	71	65	67	64
$4\nu_5$	2101	50	44	36	44	29	43
$5\nu_5$	2614	41	31	25	31	19	30
$\nu_4(\nu_6+\nu_5)$	725	48	26	42	14	42	10
$\nu_4+\nu_5(\nu_6+2\nu_5)$	1255	46	38	31	39	46	40
$\nu_4+2\nu_5(\nu_6+3\nu_5)$	1777	40	37	36	38	32	39
$\nu_4+3\nu_5(\nu_6+4\nu_5)$	2293	31	34	27	34	26	35
$2\nu_4(2\nu_6+2\nu_5)$	1435	14	4		4	5	4
$2\nu_4+\nu_5(2\nu_6+3\nu_5)$	1962	11	7	7	7	5	8
$\nu_4+\nu_6(\nu_5+2\nu_6)$		6	0.1	4	0.1	3	0.1
ν_3	1183	19	8	12	2	$\cdots$	0.1
$\nu_3+\nu_5$	1713	4	8	6	8	9	9
$\nu_3+2\nu_5$	2237	6	7	4	8	6	8
$\nu_3+\nu_4,\ \nu_2+\nu_5$ $(\nu_3+\nu_6+\nu_5)$	1905	10	1	7	2	7	2
$\nu_3+\nu_4+\nu_5,\ \nu_2+2\nu_5$ $(\nu_3+\nu_6+2\nu_5)$	2424	7	3	7	3	5	3
ν_2	1396	30	7	23	5	20	7
$\nu_9+\nu_5$	1331	4	4	$\cdots$	4	1	4
ν_6	190	61	45	117[d]	46	71[d]	69

Raman peak[a]	Raman shift[b]	309.1 nm		299.1 nm		252.7 nm		245.9 nm	
		Expt.[c]	Calc.	Expt.	Calc.	Expt.	Calc.	Expt.	Calc.
(b) Excitation wavelengths at red and blue edges of A-band absorption spectrum									
ν_5	532	1004	978	585	480	362	409	1320	1340
$2\nu_5$	1061	100	100	100	100	100	100	100	100
Absolute Raman cross section for $2\nu_5$ in Å^2/molecule (Calc)		1.61×10^{-11} (7.56×10^{-12})		3.81×10^{-11} (2.67×10^{-11})		1.08×10^{-10} (8.14×10^{-11})		5.54×10^{-11} (4.73×10^{-11})	
$3\nu_5$	1583	61	59	81	63	23	62	34	61
$4\nu_5$	2101	48	39	47	43	10	41	13	39
$5\nu_5$	2614	46	27	42	30	$\cdots$	28	$\cdots$	26
$\nu_4(\nu_6+\nu_5)$	725	71	111	64	63	70	47	183	144
$\nu_4+\nu_5(\nu_6+2\nu_5)$	1255	40	35	38	36	60	42	167	42
$\nu_4+2\nu_5(\nu_6+3\nu_5)$	1777	14	31	37	34	20	39	26	39
$\nu_4+3\nu_5(\nu_6+4\nu_5)$	2293	25	27	24	30	17	34	44	33
$2\nu_4(2\nu_6+2\nu_5)$	1435	13	3	14	3	12	4	74	4
$2\nu_4+\nu_5(2\nu_6+3\nu_5)$	1962	8	5	6	6	4	8	28	8
$\nu_4+\nu_6(\nu_5+2\nu_6)$		9	0.1	10	0.1	6	0.1	15	0.1
ν_3	1183	67	62	44	29	23	25	86	91
$\nu_3+\nu_5$	1713	4	6	7	6	15	10	21	11
$\nu_3+2\nu_5$	2237	7	5	4	6	8	9	$\cdots$	10
$\nu_3+\nu_4,\ \nu_2+\nu_5$ $(\nu_3+\nu_6+\nu_5)$	1905	15	1	15	1	4	2	11	2
$\nu_3+\nu_4+\nu_5,\ \nu_2+2\nu_5$ $(\nu_3+\nu_6+2\nu_5)$	2424	$\cdots$	2	13	2	$\cdots$	4	13	4
ν_2	1396	47	47	40	20	30	43	140	141
$\nu_9+\nu_5$	1331	$\cdots$	3	$\cdots$	4	$\cdots$	4	59	4
ν_6	190	428	251	214	100	189	267	566	740

[a]Alternative assignment of $(\nu_6+\nu_5)$ for (ν_4) is given in parentheses.
[b]Estimated uncertainties are about ±4 cm^{-1} for the Raman shifts.
[c]Relative intensities are based on integrated areas of peaks. Estimated uncertainties are about 10% for intensities 50 and higher, 20% for intensities 10–50, and 30% for intensities lower than 10.
[d]Subtraction of large Rayleigh background and solvent peaks make features below 500 cm^{-1} unreliable in the 273.9 nm and 266.0 nm spectra.

TABLE VII. Comparison of experimental and calculated resonance Raman intensities of chloroiodomethane in cyclohexane solution using the assignment of the 724 cm^{-1} peak to $\nu_5+\nu_6$.

Raman peak[a]	Raman shift[b]	282.4 nm		273.9 nm		266.0 nm	
		Expt.[c]	Calc.	Expt.	Calc.	Expt.	Calc.
(a) Excitation wavelengths at center of A-band absorption spectrum							
ν_5	532	208	132	67	37	38	20
$2\nu_5$	1061	100	100	100	100	100	100
Absolute Raman cross section for $2\nu_5$ in Å^2/molecule (Calc)		1.04×10^{-10} (9.51×10^{-11})		1.31×10^{-10} (1.31×10^{-10})		1.28×10^{-10} (1.38×10^{-10})	
$3\nu_5$	1583	84	64	71	65	67	65
$4\nu_5$	2101	50	43	36	43	29	44
$5\nu_5$	2614	41	29	25	30	19	30
$\nu_4(\nu_6+\nu_5)$	725	48	42	42	40	42	39
$\nu_4+\nu_5(\nu_6+2\nu_5)$	1255	46	41	31	39	46	38
$\nu_4+2\nu_5(\nu_6+3\nu_5)$	1777	40	36	36	35	32	34
$\nu_4+3\nu_5(\nu_6+4\nu_5)$	2293	31	31	27	31	26	29
$2\nu_4(2\nu_6+2\nu_5)$	1435	14	12	⋯	11	5	10
$2\nu_4+\nu_5(2\nu_6+3\nu_5)$	1962	11	13	7	12	5	11
$\nu_4+\nu_6(\nu_5+2\nu_6)$		6	9	4	8	3	7
ν_3	1183	19	9	12	2	⋯	0.1
$\nu_3+\nu_5$	1713	4	7	6	8	9	9
$\nu_3+2\nu_5$	2237	6	7	4	8	4	8
$\nu_3+\nu_4,\ \nu_2+\nu_5$ $(\nu_3+\nu_6+\nu_5)$	1905	10	3	7	3	7	3
$\nu_3+\nu_4+\nu_5,\ \nu_2+2\nu_5$ $(\nu_3+\nu_6+2\nu_5)$	2424	7	4	7	4	5	4
ν_2	1396	30	8	23	4	20	4
$\nu_9+\nu_5$	1331	4	4	⋯	4	1	4
ν_6	190	61	30	117[d]	3	71[d]	8

Raman peak[a]	Raman shift[b]	309.1 nm		299.1 nm		252.7 nm		245.9 nm	
		Expt.[c]	Calc.	Expt.	Calc.	Expt.	Calc.	Expt.	Calc.
(b) Excitation wavelengths at red and blue edges of A-band absorption spectrum									
ν_5	532	1004	1028	585	503	362	397	1320	1294
$2\nu_5$	1061	100	100	100	100	100	100	100	100
Absolute Raman cross section for $2\nu_5$ in Å^2/molecule (Calc)		1.61×10^{-11} (7.11×10^{-12})		3.81×10^{-11} (2.48×10^{-11})		1.08×10^{-10} (8.53×10^{-11})		5.54×10^{-11} (4.97×10^{-11})	
$3\nu_5$	1583	61	56	81	60	23	64	34	62
$4\nu_5$	2101	48	34	47	39	10	43	13	41
$5\nu_5$	2614	46	22	42	26	⋯	29	⋯	28
$\nu_4(\nu_6+\nu_5)$	725	71	48	64	46	70	36	183	35
$\nu_4+\nu_5(\nu_6+2\nu_5)$	1255	40	41	38	42	60	35	167	33
$\nu_4+2\nu_5(\nu_6+3\nu_5)$	1777	14	34	37	37	20	31	26	29
$\nu_4+3\nu_5(\nu_6+4\nu_5)$	2293	25	28	24	31	17	27	44	25
$2\nu_4(2\nu_6+2\nu_5)$	1435	13	13	14	13	12	8	78	8
$2\nu_4+\nu_5(2\nu_6+3\nu_5)$	1962	8	14	6	14	4	10	28	9
$\nu_4+\nu_6(\nu_5+2\nu_6)$		9	10	10	10	6	6	15	6
ν_3	1183	67	66	44	31	23	24	86	88
$\nu_3+\nu_5$	1713	4	6	7	6	15	10	21	11
$\nu_3+2\nu_5$	2237	7	5	4	6	8	9	⋯	10
$\nu_3+\nu_4,\ \nu_2+\nu_5$ $(\nu_3+\nu_6+\nu_5)$	1905	15	2	15	3	4	3	11	4
$\nu_3+\nu_4+\nu_5,\ \nu_2+2\nu_5$ $(\nu_3+\nu_6+2\nu_5)$	2424	⋯	3	13	3	⋯	5	13	5
ν_2	1396	47	54	40	24	30	38	140	134
$\nu_9+\nu_5$	1331	⋯	3	⋯	4	⋯	4	59	4
ν_6	187	428	387	214	167	189	189	566	604

[a]Alternative assignment of $(\nu_6+\nu_5)$ for (ν_4) is given in parentheses.
[b]Estimated uncertainties are about ±4 cm^{-1} for the Raman shifts.
[c]Relative intensities are based on integrated areas of peaks. Estimated uncertainties are about 10% for intensities 50 and higher, 20% for intensities 10–50, and 30% for intensities lower than 10.
[d]Subtraction of large Rayleigh background and solvent peaks make features below 500 cm^{-1} unreliable in the 273.9 nm and 266.0 nm spectra.
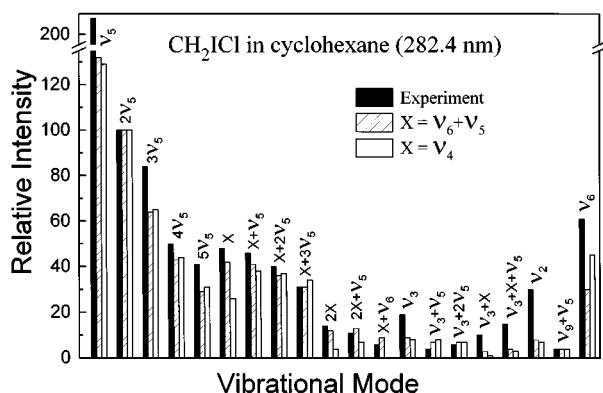
FIG. 6. Comparison of experimental (solid bar) and calculated (dashed bar for $\nu_5+\nu_6$ assignment and open bar of ν_4 assignment) resonance Raman intensities for the 282.4 nm h_2-chloroiodomethane resonance Raman spectrum. The calculated resonance Raman intensities made use of the parameters in Table V in Eqs. (2)–(10) and the model described in Sec. III.
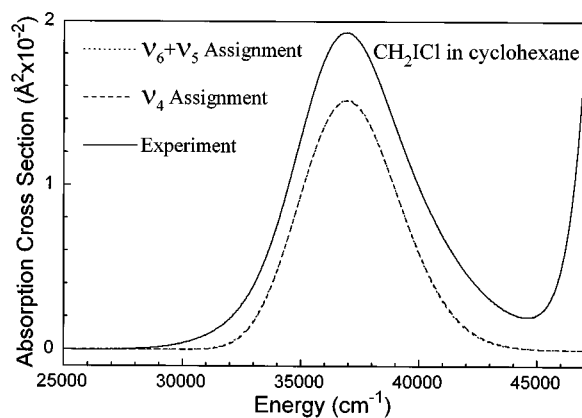

FIG. 7. Comparison of experimental (solid line) and calculated (dotted line for $\nu_5+\nu_6$ assignment and dashed line for ν_4 assignment) A-band absorption spectra. The calculated absorption spectra made use of the parameters in Table V in Eqs. (2)–(10) and the model described in Sec. III.

excitation wavelengths, particularly for the wavelengths near the center of the A-band absorption (282.4 nm, 273.9 nm, and 266.0 nm) where we expect the $^3Q_0$ transition to give the dominate contribution to the A-band absorption. Our calculated absolute Raman cross sections are somewhat lower than the experimental cross sections for the 299.1 nm and 309.1 nm resonance Raman spectra and this could be due to the calculations not taking into account the contribution of the $^3Q_1$ state which is expected to be important in the red-edge part of the A-band absorption. Similarly, the calculated absolute Raman cross sections are lower than the experimental cross section at 252.7 nm and this could be due to neglecting the contribution of the $^1Q_1$ state which is expected to be important in the blue-edge part of the A-band absorption. Figure 7 compares the experimental and calculated absorption spectra of h_2-chloroiodomethane. The calculated absorption spectra in Fig. 7 display relatively good agreement with the experimental absorption spectra bearing in mind that we have neglected the small contributions of the $^3Q_1$ and $^1Q_1$ states to the red and blue edges of the A-band absorp-

tion. Table VIII gives the parameters for calculating the fully deuterated chloroiodomethane absorption spectrum and resonance Raman intensities using both the ν_4 and the $\nu_5+\nu_6$ assignments for the 724 cm^{-1} Raman peak. Table IX and Fig. 8 compare the calculated and experimental 282.4 nm resonance Raman intensities for d_2-chloroiodomethane and there appears to be reasonably good agreement for most Raman lines. Figure 9 displays the comparison of the calculated and experimental absorption spectra for d_2-chloroiodomethane and the agreement is similar to that observed for the fully protonated chloroiodomethane in Fig. 7.

In general, the calculated resonance Raman intensities for both possible assignments of the 724 cm^{-1} Raman peak to either the ν_4 fundamental or the $\nu_6+\nu_5$ combination band show reasonable agreement with the experimental intensities. However, the $\nu_6+\nu_5$ combination band assignment for the 724 cm^{-1} Raman peak does a noticeable better job of fitting several Raman lines compared compared to the ν^4 fundamental assignment. In particular, the $\nu_6+\nu_5$ combination

TABLE VIII. Parameters for calculation of resonance Raman intensities and absorption spectrum of d_2-chloroiodomethane in cyclohexane solution.

Vibrational mode	Ground state vibrational frequency (cm^{-1})	Excited state vibrational frequency (cm^{-1})	$|\Delta|$
(a) Using assignment of 724 cm^{-1} peak to ν_4			
ν_5 (C–I stretch)	509 cm^{-1}	509 cm^{-1}	4.95
ν_4 (C–Cl stretch)	709 cm^{-1}	709 cm^{-1}	1.40
ν_3 (CH$_2$ wag)	891 cm^{-1}	891 cm^{-1}	1.15
ν_6 (Cl–C–I bend)	190 cm^{-1}	190 cm^{-1}	0.50
Transition length, $M=0.191$ Å			
$E_0=29\,700$ cm^{-1}			
(b) Using assignment of 724 cm^{-1} peak to $\nu_5+\nu_6$			
ν_5 (C–I stretch)	509 cm^{-1}	509 cm^{-1}	4.95
ν_6 (Cl–C–I bend)	190 cm^{-1}	190 cm^{-1}	4.9
ν_3 (CH$_2$ wag)	891 cm^{-1}	891 cm^{-1}	1.15
Transition length, $M=0.191$ Å			
$E_0=28\,100$ cm^{-1}			

TABLE IX. Comparison of calculated and experimental resonance Raman intensities of deuterated chloroiodomethane in cyclohexane solution.

Raman peak[a]	Raman shift (cm^{-1})[b]	282.4 nm intensity[c]	Calc. using ν_4 assignment	Calc. using $\nu_5+\nu_6$ assignment
ν_5	505	165	173	173
$2\nu_5$	1004	100	100	100
Absolute Raman cross section for $2\nu_5$ in $Å^2$/molecule		Expt.$=1.02\times10^{-10}$ (Calc.)$=$	(1.02×10^{-10})	(1.03×10^{-10})
$3\nu_5$	1499	52	63	63
$4\nu_5$	1991	25	42	42
$5\nu_5$	2476	12	29	28
$\nu_4(\nu_6+\nu_5)$	697	43	43	30
$\nu_4+\nu_5(\nu_6+2\nu_5)$	1196	29	29	29
$\nu_4+2\nu_5(\nu_6+3\nu_5)$	1691	28	27	25
$\nu_4+3\nu_5(\nu_6+4\nu_5)$ and ν_1	2191	25[d]	24	22
ν_3	892	70	70	70
$\nu_3+\nu_5$	1393	39	29	29
$\nu_3+2\nu_5$	1891	22	27	27
$\nu_3+3\nu_5$	2385	15	24	23
$\nu_3+\nu_4$ $(\nu_3+\nu_6+\nu_5)$	1586	10	4	8
$\nu_3+\nu_4+\nu_5$ $(\nu_3+\nu_6+\nu_5)$	2079	4	8	11
$\nu_3+\nu_4+2\nu_5$ $(\nu_3+\nu_6+3\nu_5)$	2572	5	10	12
ν_6	191	131	131	131

[a]Alternative assignment of $(\nu_6+\nu_5)$ for (ν_4) is given in parentheses.
[b]Estimated uncertainties are about ±4 cm^{-1} for the Raman shifts.
[c]Relative intensities are based on integrated areas of peaks. Estimated uncertainties are about 10% for intensities 50 and higher, 20% for intensities 10–50, and 30% for intensities lower than 10.
[d]Two peaks contribute to this intensity (the nominal C–D stretch, ν_1, and either $\nu_4+3\nu_5$ or $\nu_6+4\nu_5$).

band assignment calculations fits the experimental intensities of the $\nu_6+\nu_5$ combination band (or the ν_4 fundamental in the other assignment possibility) and the $2\nu_6+\nu_5$ combination band (or the $\nu_4+\nu_6$ line in the other assignment possibility). We note that if the ν_4 assignment is probable and wee see $\nu_4+\nu_6$ in our spectra then we would also likely see $\nu_5+\nu_6$. This suggests that the 724 cm^{-1} Raman peak and its associated combination bands in our resonance Raman spectra may

be mostly due to the $\nu_6+n\nu_5$ combination bands rather than the $\nu_4+n\nu_5$ combination bands.

We have carried out calculations with and without the preresonant contribution for the fundamental intensities in order to compare these values with the experimental intensities. Figure 10 displays the experimental absolute resonance Raman intensities for the nominal C–I stretch fundamental (ν_5) and the calculated absolute Raman intensities with and
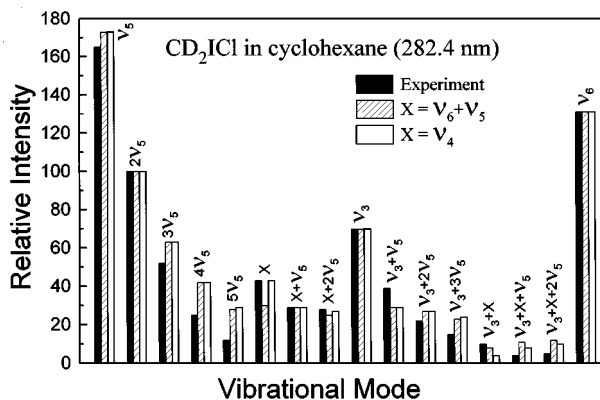

FIG. 8. Comparison of experimental (solid bar) and calculated (dashed bar for $\nu_5+\nu_6$ assignment and open bar for ν_4 assignment) resonance Raman intensities for the 282.4 nm d_2-chloroiodomethane resonance Raman spectrum. The calculated resonance Raman intensities made use of the parameters in Table VIII in Eqs. (2)–(10) and the model described in Sec. III.
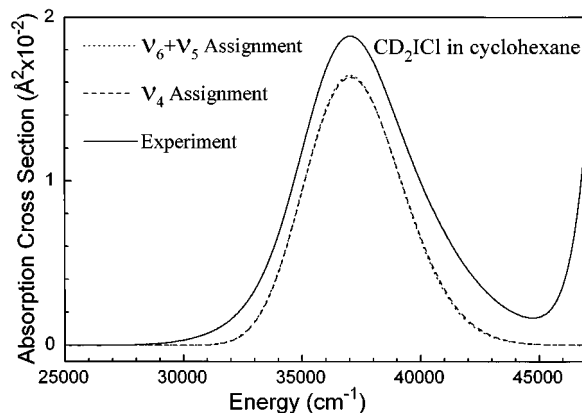

FIG. 9. Comparison of experimental (solid line) and calculated (dotted line for $\nu_5+\nu_6$ assignment and dashed line for ν_4 assignment) A-band absorption spectra of d_2-chloroiodomethane. The calculated absorption spectra made use of the parameters in Table VIII in Eqs. (2)–(10) and the model described in Sec. III.
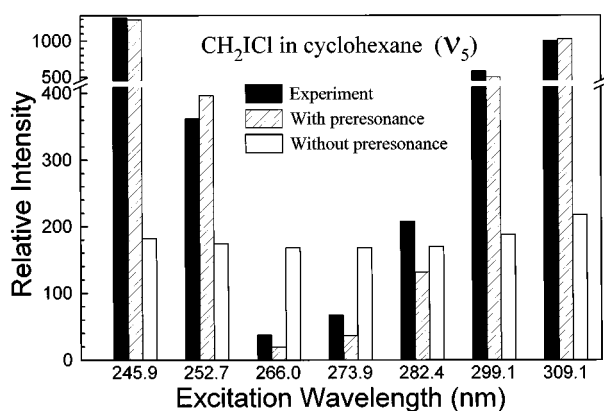
FIG. 10. Comparison of the experimental (solid bars) and calculated (dashed bar for calculations with preresonant contribution and open bar for calculations without preresonant contribution) Raman intensities for the ν_5 nominal C–I stretch fundamental.

without the preresonant contribution to the fundamental intensities taken into account. Figure 10 clearly shows that the calculations with the preresonant contribution agree much better with the experimental intensities than the calculations which have no preresonant contribution. This illustrates the importance of resonance–preresonance interferences in elucidating the fundamental intensities within resonance Raman spectra associated with a weak absorption band which has very strong absorption transitions nearby.

E. Photodissociation dynamics

In order to examine the short-time photodissociation dynamics of chloroiodomethane in terms of easily visualized internal coordinates, we use the dimensionless normal mode displacements from our simulations and the normal-mode descriptions in Eqs. (11) and (12) to obtain the change in the internal coordinates as a function of time after photoexcitation. Since the overlaps $\langle f|0(t)\rangle$ that determine the calculated resonance Raman intensities generally reach their maxima around 5–10 fs, we have chosen 10 fs as the time which we will examine the photodissociation dynamics. We also note that at 10 fs the nuclei have not moved very far from the Franck–Condon region and 10 fs is relatively short with respect to the recurrence times of the Franck–Condon active vibrations. Because our resonance Raman intensity analysis only gives us the magnitude of the normal-coordinate displacements, we need some way to determine the signs of the normal mode displacements (Δ). The reader is referred to several recent review articles[67,82] on resonance Raman intensity analysis for a more thorough discussion of the problem of choosing the signs of the normal mode displacements. For the purpose of investigating the short-time photodissociation dynamics of chloroiodomethane, we will use a combination of chemical intuition and the redundancy found in the resonance Raman intensities of isotopic derivatives.

Since we know that the C–I bond is broken in an apparently direct photodissociation, we shall assume that the C–I

bond becomes longer upon excitation and this makes the normal mode displacement for the nominal C–I stretch positive in sign. This eliminates half of the 2^n possible sign combinations (for n Franck–Condon active modes) for the normal mode displacements. We will further reduce the number of possible sign combinations that we need to consider by comparing resonance Raman data of both h_2-chloroiodomethane and d_2-chloroiodomethane. The geometry change(s) with least variance across the set of isotopic derivatives should yield the most probable excited-state geometry changes because the electronic structure is assumed to be isotope invariant. For each possible sign combination of normal mode displacements we use Eqs. (11) and (12) to generate a different excited-state geometry at 10 fs and the excited-state geometry(ies) which have the smallest variance between the h_2-chloroiodomethane and d_2-chloroiodomethane derivatives will be selected as the most probable. We find that there are three possible excited-state geometries for the $\nu_5+\nu_6$ assignment that have rms differences between the d_2- and h_2-chloroiodomethane derivatives that are significantly lower than any of the others (by factors of 1.8 or more) and we pick these as the only realistic possibilities. For the ν_4 assignment, we make an additional assumption that the C–Cl bond becomes larger. This seems reasonable since if the ν_4 is really Franck–Condon active in the A-band it is most likely due to some coupling of the C–Cl stretch and C–I stretch chromophores which both have $n \text{-}>\sigma^*$ transitions that lead to the C–X bond being broken in the lowest absorption bands of the monohalomethanes. For the ν_4 assignment we find four possible excited-state geometries that have rms differences between the d_2- and h_2-chloroiodomethane derivatives that are significantly lower than any of the others (by factors of 1.7 or more) and we choose these as the only realistic possibilities. Table X shows the range of internal coordinate changes found at 10 fs for the most probable normal mode sign combinations of the $\nu_5+\nu_6$ assignment (three sign combinations) and the ν_4 assignment (four sign combinations). Figure 11 shows the geometry of chloroiodomethane which can be used to help visualize the internal coordinate changes given in Table X.

Examination of Table X shows that the short-time photodissociation dynamics of the two different assignment possibilities for the 724 cm^{-1} Raman peak are very similar to one another. This is not unexpected since the dominant progression in the chloroiodomethane resonance Raman spectra is the nominal C–I stretch overtone progression and this may be expected to dominate the overall photodissociation dynamics. The ambiguity of the assignment of the 724 cm^{-1} Raman band and its associated combination band progression shows up primarily in the amount of change in the C–Cl internal coordinate; the ν_4 assignment gives a large change in the C–Cl bond length during the short-time photodissociation dynamics while the $\nu_5+\nu_6$ assignment gives a much smaller change in the C–Cl bond length. Even with this ambiguity in the amount of the C–Cl bond length changes, we can learn a great deal about the short-time photodissociation dynamics of chloroiodomethane upon excitation in the A-band absorption. During the first 10 fs the C–I bond

TABLE X. Most probable internal coordinate displacements of chloroiodomethane at $t=10$ fs assuming the C–I bond becomes longer.

	Range of displacements at 10 fs	
Internal coordinate	Using ν_4 assignment[a]	Using $\nu_5+\nu_6$ assignment[b]
C–H bonds	<0.01 Å	<0.01 Å
C–I bond, atoms 1 and 4	$+0.141$ Å to $+0.142$ Å	$+0.157$ Å to $+0.171$ Å
C–Cl bond, atoms 1 and 5	$+0.068$ Å to $+0.069$ Å	-0.020 Å to -0.024 Å
H–C–H angle, atoms 2, 1, and 3	$-0.6°$ to $-0.7°$	$-1.1°$ to $-2.4°$
H–C–I angle, atoms 2, 1, and 4	$-0.5°$ to $-5.1°$	$-2.5°$ to $-7.5°$
H–C–Cl angle, atoms 2, 1, and 5	$+5.4°$ to $+8.6°$	$+7.2°$ to $+10.5°$
H–C–I angle, atoms 3, 1, and 4	$-0.5°$ to $-5.1°$	$-2.5°$ to $-7.5°$
H–C–Cl angle, atoms 3, 1, and 5	$+5.4°$ to $+8.6°$	$+7.3°$ to $+10.5°$
I–C–Cl angle, atoms 4, 1, and 5	$-8.0°$ to $-8.2°$	$-5.0°$ to $-7.3°$

[a]Values are for four most probable sign combinations of the normal mode displacements (see text).
[b]Values are for three most probable sign combinations of the normal mode displacements (see text).

lengthens by 0.157–0.171 Å for the $\nu_5+\nu_6$ assignment or about 0.142 Å for the ν_4 assignment. The Cl–C–I angle becomes smaller by -5.0 to -7.3 deg for the $\nu_5+\nu_6$ assignment or about -8.0 to -8.2 deg for the ν_4 assignment. The H–C–I angles become smaller by -2.5 to -7.5 deg for the $\nu_5+\nu_6$ assignment or -0.5 to -5.1 deg for the ν_4 assignment. The H–C–Cl angles become larger by $+7.2$ to $+10.5$ deg for the $\nu_5+\nu_6$ assignment or $+5.4$ to $+8.6$ deg for the ν_4 assignment. The C–I bond length changes, the CI–C–I angles changes, the H–C–I angle changes, and the H–C–Cl angle changes are all qualitatively consistent with a ''soft'' radical model[83] of photodissociation dynamics in which the carbon atom is pushed into the departing radical. These dynamics are also consistent with the CH_2Cl group changing towards a more planar geometry and we note that the ground state of CH_2Cl radicals formed in matrix isolation experiments are most likely planar.[84,85] However, the H–C–H angle change of -1.1 to -2.4 deg for the $\nu_5+\nu_6$ assignment or about -0.6 deg for the ν_4 assignment is not qualitatively consistent with the ''soft'' radical impulsive model[83] of photodissociation dynamics which would predict that the H–C–H angle should increase. One would also expect that the H–C–H angle should become larger as it goes toward a planar geometry of ground state CH_2Cl radicals. This appears to suggest that the H–C–H angle moves toward the ground state planar structure of the CH_2Cl radical substantially slower than the H–C–Cl angles. Why does the simple impulsive ''soft'' radical model do a poor job in describing the H–C–H motion? The ''soft'' radical model in its simplest form[83] assumes that all of the radical atoms are very loosely bound to one another to approximately the same extent and does not take into account the force constants or ''stiffness'' of the different bonds in the radical to be formed from the bond breaking process. Examination of Table X shows that there is very little change in the C–H bond lengths at 10 fs. The C–H stretch motion has a higher frequency and greater stiffness than the lower frequency motions associated with the C, Cl, and I atoms. Similarly, the H–C–H bend motion has a somewhat higher frequency than the H–C–l and H–C–Cl motions. It appears that as the C–I bond starts to break in the A-band chloroiodomethane pho-

todissociation, the C–H stretch and H–C–H bend motions are relatively uncoupled from the lower frequency motions associated with the C–I stretch, C–Cl stretch, Cl–C–I bend, H–C–l bend, and H–C–Cl bend internal coordinates and this results in very small changes in the C–H bond length and H–C–H angle during the initial stages of the photodissociation compared to the other internal coordinates which are associated with lower frequency motions. The short-time photodissociation dynamics appear to be more consistent with a model that has the C–I bond breaking pushing into a semirigid radical (with appropriate force constants for the radical group) similar to an impulsive model suggested by Riley and Wilson on p. 143 of Ref. 83.

The results from the resonance Raman intensity analysis only describes the Franck–Condon region of the excited-state surface and the initial photodissociation dynamics, while the product state distributions of the photoproducts depend on the complete excited-state potential energy surface out to the asymptotic limit. The ambiguity of the assignment of the 724 cm^{-1} Raman peak and its associated combination bands in our resonance Raman spectra limits what we can learn about the coupling of the C–Cl and C–I chromophores and our results only provide upper and lower limits on the changes of the C–Cl bond length in the initial photodissociation dynamics. The amount of the C–Cl bond length changes during the photodissociation is probably a fairly sensitive measure of the amount of coupling of the C–Cl and C–I chromophores in the A-band absorption. In order to pinpoint the amount of coupling in this weak coupling case, there are several types of experiments that may be done to more accurately determine the amount of C–Cl and C–I coupling. Substantially higher resolution resonance Raman experiments on low pressure gases may be able to resolve the assignment and the relative contributions of the two possible series of peaks ($\nu_4+n\nu_5$ and $\nu_6+n\nu_5$) that may compose the 724 cm^{-1} Raman peak and its associated combination bands observed in our relatively low resolution solution phase spectra. To the extent that the initial photodissociation dynamics determine the photoproduct state distributions, it may be useful to attempt infrared emission, anti-Stokes resonance Raman scattering, and multiphoto-
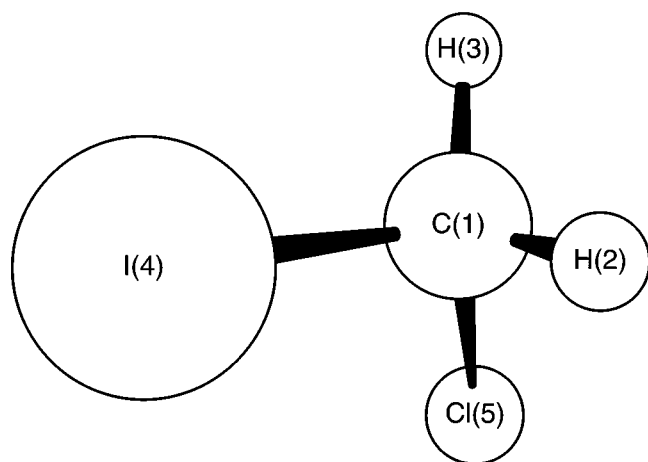
FIG. 11. Geometry of chloroiodomethane with each atom labeled with a number 1–5.

nionization (MPI) experiments to find the degree of vibrational excitation of the C–Cl bond in the CH_2Cl radical formed from the A-band photodissociation.

Our computational simulations of the resonance Raman intensities of chloroiodomethane in the A-band indicate that the Raman intensities observed in our experimental spectra are determined by the first 20–30 fs of excited-state dynamics. This time for the excited-state dynamics is substantially shorter than typical dielectric relaxation times or collisional times in the solution phase. We therefore expect that the resonance Raman spectra (and absorption spectra) will be mostly sensitive to static changes (mean-field effects) of the potential energy surfaces and we can consider the solvent molecules to be almost ''frozen'' during the time needed to determine the resonance Raman intensities and absorption spectrum. During the later stages of the C–I bond breaking when the CH_2Cl and I fragments have separated substantially, we expect that dynamical solvent effects will become more noticeable. Our successful modeling of both the absolute and relative resonance Raman intensities without including any additional damping term besides motion of the wave packet out of the Franck–Condon region strongly suggests that the spectra are determined by dynamics taking place on a time scale shorter than any electronic dephasing due to dielectric friction or solvent collisional effects. We also note that we do not observe any appreciable broad fluorescence background underneath our experimental resonance Raman spectra and this also implies that the resonance Raman spectra are mostly sensitive to the static and not dynamical solvent–solute interactions. The directly dissociative nature of the C–I bond breaking causes the wave packet to leave the Franck–Condon region very rapidly (less than 50 fs based on our modeling of the resonance Raman intensities). In molecules that are not directly dissociative, the excited-state amplitude usually stays near the Franck–Condon region long enough to change the optically made coherent superposition of states into an incoherent population of states on the excited-state potential energy surface which then emits a broad fluorescence spectrum. For example, solution phase

CS_2 has an excited-state lifetime on the order of a few picoseconds and its resonance Raman spectrum is superimposed upon a broad fluorescence spectrum.[66]

V. CONCLUSIONS

We have presented postresonance and resonance Raman spectra of h_2-chloroiodomethane in cyclohexane solution taken with fourteen excitation wavelengths within and above the A-band absorption and a 282.4 nm resonance Raman spectrum of d_2-chloroiodomethane. We have also measured the absolute Raman cross sections for all of the presented resonance Raman spectra. We have used a simple model which includes preresonant contributions to the fundamental intensities to simulate the resonance Raman intensities and absorption spectra of h_2-chloroiodomethane and d_2-chloroiodomethane. The description of the normal mode vibrations was used together with the results of the time-dependent wave packet calculations to find the short-time photodissociation dynamics in easily visualized internal coordinate motions. In the initial stages of the photodissociation the C–I bond lengthens, the I–C–Cl and H–C–I angles becomes smaller, the H–C–Cl angles become larger, and the H–C–H angle becomes smaller by a slight amount. The C–H bond does not change much and an ambiguity in the assignment of the 724 cm^{-1} Raman peak and its combination bands to either the $\nu_4 + n\nu_5$ and the $\nu_6 + n\nu_5$ progressions limits what we can determine about the C–Cl bond length changes during the initial stages of the photodissociation. Most of the short-time photodissociation dynamics are consistent with an impulsive ''soft'' radical model of the photodissociation dynamics except the higher frequency C–H stretch and H–C–H bend motions which appear relatively uncoupled from the low frequency motions associated with the Franck–Condon active modes. We note that the H–C–I, I–C–Cl, and H–C–Cl bending motions during the short-time photodissociation dynamics are all consistent with the CH_2Cl group becoming more planar.

Future work will involve experiments to map out a more complete excitation profile and developing better models for describing the resonance Raman intensities and absorption spectra in order to help elucidate the relative contributions and locations of the $^3Q_0$, $^3Q_1$, and $^1Q_1$ transitions as well as the short-time photodissociation dynamics of the $^3Q_1$, and $^1Q_1$ states.

ACKNOWLEDGMENTS

[1] E. J. Heller, J. Chem. Phys. **62**, 1544 (1975).
[2] S. Y. Lee and E. J. Heller, J. Chem. Phys. **71**, 4777 (1979).
[3] E. J. Heller, Acc. Chem. Res. **14**, 368 (1981).
[4] E. J. Heller, R. L. Sundberg, and D. J. Tannor, J. Phys. Chem. **86**, 1822 (1982).

[5] A. B. Myers, R. A. Mathies, D. J. Tannor, and E. J. Heller, J. Chem. Phys. **77**, 3857 (1982).

[6] D. G. Imre, J. L. Kinsey, R. W. Field, and D. H. Katayama, J. Phys. Chem. **86**, 1822 (1982).

[7] D. G. Imre, J. L. Kinsey, A. Sinha, and J. Krenos, J. Phys. Chem. **88**, 3956 (1984).

[8] M. O. Hale, G. E. Galica, S. G. Glogover, and J. L. Kinsey, J. Phys. Chem. **90**, 4997 (1986).

[9] G. E. Galica, B. R. Johnson, J. L. Kinsey, and M. O. Hale, J. Phys. Chem. **95**, 7994 (1991).

[10] K. Q. Lao, M. D. Person, P. Xayaroboun, and L. J. Butler, J. Chem. Phys. **92**, 823 (1990).

[11] F. Markel and A. B. Myers, Chem. Phys. Lett. **167**, 175 (1990).

[12] A. B. Myers and F. Markel, Chem. Phys. **149**, 21 (1990).

[13] F. Markel and A. B. Myers, J. Chem. Phys. **98**, 21 (1993).

[14] P. G. Wang and L. D. Ziegler, J. Phys. Chem. **97**, 3139 (1993).

[15] E. A. Rolfing and J. J. Valentini, Chem. Phys. Lett. **114**, 282 (1985).

[16] E. A. Rolfing and J. J. Valentini, J. Chem. Phys. **83**, 521 (1985).

[17] R. J. Sension, R. J. Brudzynski, and B. S. Hudson, Phys. Rev. Lett. **61**, 694 (1988).

[18] R. J. Sension, R. J. Brudzynski, B. S. Hudson, J. Z. Zhang, and D. G. Imre, Chem. Phys. **141**, 393 (1990).

[19] J. Zhang and D. G. Imre, J. Chem. Phys. **89**, 309 (1988).

[20] W. M. Kwok and D. L. Phillips, Chem. Phys. Lett. **241**, 260 (1995).

[21] W. M. Kwok and D. L. Phillips, J. Chem. Phys. **104**, 2529 (1996).

[22] K. Klienermans, E. Linnebach, and R. J. Suntz, J. Phys. Chem. **91**, 5543 (1987).

[23] M. D. Person, K. Q. Lao, B. J. Eckholm, and L. J. Butler, J. Chem. Phys. **91**, 812 (1989).

[24] R. J. Brudzynski, R. J. Sension, and B. S. Hudson, Chem. Phys. Lett. **165**, 487 (1990).

[25] K. Q. Lao, E. Jensen, P. W. Kash, and L. J. Butler, J. Chem. Phys. **93**, 3958 (1990).

[26] D. L. Phillips and A. B. Myers, J. Phys. Chem. **95**, 7164 (1991).

[27] P. W. Browning, E. Jensen, G. C. G. Waschewsky, M. R. Tate, L. J. Butler, and J. P. Hessler, J. Chem. Phys. **101**, 5652 (1994).

[28] D. L. Phillips, B. A. Lawrence, and J. J. Valentini, J. Phys. Chem. **95**, 7570 (1991).

[29] D. L. Phillips, B. A. Lawrence, and J. J. Valentini, J. Phys. Chem. **95**, 9085 (1991).

[30] D. L. Phillips and A. B. Myers, J. Chem. Phys. **95**, 226 (1991).

[31] D. L. Phillips, J. J. Valentini, and A. B. Myers, J. Phys. Chem. **96**, 2039 (1992).

[32] D. L. Phillips and W. M. Kwok, Chem. Phys. Lett. **241**, 267 (1995).

[33] S. Q. Man, W. M. Kwok, and D. L. Phillips, J. Phys. Chem. **99**, 15 705 (1995).

[34] R. J. Sension and H. L. Strauss, J. Chem. Phys. **85**, 3791 (1986).

[35] J. Xu, N. Schwentner, and M. Chergui, J. Chem. Phys. **101**, 7381 (1994).

[36] J. Xu, N. Schwentner, S. Hennig, and M. Chergui, J. Chim. Phys. **92**, 541 (1995).

[37] J. Strempel and W. Kiefer, J. Chem. Phys. **95**, 2391 (1991).

[38] M. Ganz, J. Strempel, and W. Kiefer, Chem. Phys. Lett. **207**, 110 (1993).

[39] A. E. Johnson and A. B. Myers, J. Chem. Phys. **102**, 3519 (1995).

[40] A. Gedanken and M. D. Rowe, Chem. Phys. Lett. **34**, 39 (1975).

[41] M. Dzvonik, S. Yang, and R. Bersohn, J. Chem. Phys. **61**, 4408 (1974).

[42] J. F. Black and I. Powis, Chem. Phys. **125**, 375 (1988).

[43] L. R. Khundar and A. H. Zewail, Chem. Phys. Lett. **142**, 426 (1987).

[44] R. K. Sparks, K. Shobatke, L. R. Carlson, and Y. T. Lee, J. Chem. Phys. **75**, 3838 (1981).

[45] G. N. A. Van Veen, T. Baller, A. E. de Vries, and N. J. A. van Veen, Chem. Phys. **87**, 405 (1984).

[46] I. Powis and J. F. Black, J. Phys. Chem. **93**, 2461 (1989).

[47] R. Ogorzalek-Loo, H.-P. Haerri, G. E. Hall, and P. L. Houston, J. Chem. Phys. **90**, 4222 (1989).

[48] D. W. Chandler, M. H. M. Janssen, S. Stolte, R. N. Strickland, J. W. Thoman, and D. H. Parker, J. Phys. Chem. **94**, 4839 (1990).

[49] G. E. Hall, T. J. Sears, and J. M. Frye, J. Chem. Phys. **89**, 580 (1988).

[50] N. E. Triggs, M. Zahedi, J. W. Nibler, P. A. DeBarber, and J. J. Valentini, J. Chem. Phys. **96**, 1822 (1992).

[51] P. Brewer, P. Das, G. Ondrey, and R. Bersohn, J. Chem. Phys. **79**, 720 (1983).

[52] W. P. Hess, S. J. Kohler, H. K. Haugen, and S. R. Leone, J. Chem. Phys. **84**, 2143 (1986).

[53] Q. Zhu, J. R. Cao, Y. Wen, J. Zhang, Y. Haung, W. Fang, and X. Wu, Chem. Phys. Lett. **144**, 486 (1988).

[54] M. Shapiro and R. Bersohn, J. Chem. Phys. **72**, 3810 (1980).

[55] S. K. Gray and M. S. Child, Mol. Phys. **51**, 189 (1984).

[56] M. Shapiro, J. Phys. Chem. **90**, 3644 (1986).

[57] M. Tadjeddine, J. P. Flament, and C. Teichteil, Chem. Phys. **118**, 45 (1987).

[58] H. Guo and G. C. Schatz, J. Chem. Phys. **93**, 393 (1990).

[59] Y. Amatsu, K. Morokuma, and S. Yabushita, J. Chem. Phys. **94**, 4858 (1991).

[60] H. Guo and G. C. Schatz, J. Chem. Phys. **95**, 3091 (1991).

[61] H. Guo, J. Chem. Phys. **96**, 2731 (1992).

[62] G. Schmitt and F. J. Comes, J. Photochem. A **41**, 13 (1987).

[63] S. J. Lee and R. Bersohn, J. Chem. Phys. J. Phys. Chem. **86**, 728 (1982).

[64] L. J. Butler, E. J. Hintsa, and Y. T. Lee, J. Chem. Phys. **84**, 4104 (1986).

[65] L. J. Butler, E. J. Hintsa, S. F. Shane, and Y. T. Lee, J. Chem. Phys. **86**, 2051 (1987).

[66] A. B. Myers, B. Li, and X. Ci, J. Chem. Phys. **89**, 1876 (1988).

[67] A. B. Myers, in *Laser Techniques in Chemistry*, edited by A. B. Myers and T. R. Rizzo (Wiley, New York, 1995), p. 325.

[68] P. Stein, V. Miskowski, W. H. Woodruff, J. P. Griffin, K. G. Werner, B. P. Gaber, and T. G. Spiro, J. Chem. Phys. **64**, 2159 (1976).

[69] G. M. Korenowski, L. D. Ziegler, and A. C. Albrecht, J. Chem. Phys. **68**, 1248 (1978).

[70] G. A. Schick and D. F. Bocian, J. Raman Spectrosc. **11**, 27 (1981).

[71] S. A. Asher and C. R. Johnson, J. Phys. Chem. **89**, 1375 (1985).

[72] S. P. A. Fodor, R. A. Copeland, C. A. Grygon, and T. G. Spiro, J. Am. Chem. Soc. **111**, 5509 (1989).

[73] I. W. Sztainbuch and G. E. Leroi, J. Chem. Phys. **93**, 4642 (1990).

[74] K.-S. K. Shin and J. I. Zink, J. Am. Chem. Soc. **112**, 7148 (1990).

[75] A. C. Albrecht and M. C. Hutley, J. Chem. Phys. **55**, 4438 (1971).

[76] B. U. Curry, Ph.D. dissertation, University of California, Berkeley, 1983.

[77] I. Ohkoshi, Y. Nide, and M. Takano, J. Mol. Spectrosc. **124**, 118 (1987).

[78] (a) M. Zaki El-Sabban, A. Danti, and B. J. Zwolinski, J. Chem. Phys. **44**, 1770 (1966); (b) see AIP document No. PAPS JCPSA-9816-6 for 6 pages of tables. Order by PAPS number and journal reference from American Institute of Physics, Physics Auxiliary Publication Service, Carolyn Gehlbach, 500 Sunnyside Boulevard, Woodbury, New York 11797-2999. Fax: 516-576-2223, e-mail: janis@aip.org. The price is $1.50 for each microfiche (98 pages) or $5.00 for photocopies of up to 30 pages, and $0.15 for each additional page over 30 pages. Airmail additional. Make checks payable to the American Institute of Physics.

[79] B. H. Torrie, D. A. Prystupa, J. Clark, S. Taylor, and Y. W. Wong, J. Raman Spectrosc. **21**, 423 (1990).

[80] V. Sablinskas, P. Klaboe, C. J. Nielsen, and D. Sülzle, Analyst **117**, 365 (1992).

[81] E. B. Wilson, Jr., J. C. Decius, and P. C. Cross, *Molecular Vibrations* (Dover, New York, 1980).

[82] A. B. Myers and R. A. Mathies, in *Biological Applications of Raman Spectroscopy*, edited by T. G. Spiro (Wiley, New York, 1987), Vol. 2, p. 1.

[83] S. J. Riley and K. R. Wilson, Faraday Discuss. Chem. Soc. **53**, 132 (1972).

[84] D. W. Smith and L. Andrews, J. Chem. Phys. **55**, 5295 (1971).

[85] D. W. Smith and L. Andrews, Spectrochim. Acta **28A**, 493 (1972).